

TRI-PP-04-10

Effective field theory on the deuteron with dibaryon field

Shung-ichi Ando ^{a,1} and Chang Ho Hyun ^{b,c,2}

^a *Theory Group, TRIUMF, 4004 Wesbrook Mall, Vancouver, B.C. V6T 2A3, Canada*

^b *School of Physics, Seoul National University, Seoul 151-742, Korea*

^c *Institute of Basic Science, Sungkyunkwan University, Suwon 440-746, Korea*

Pionless effective field theory with dibaryon fields is reexamined for observables involving the deuteron. The electromagnetic form factors of the deuteron and the total cross sections of radiative neutron capture on the proton, $n p \rightarrow d \gamma$, are calculated. The low energy constants of vector(photon)-dibaryon-dibaryon vertices in the effective lagrangian are fixed primarily by the one-body vector(photon)-nucleon-nucleon interactions. This scheme for fixing the values of the low energy constants satisfactorily reproduces the results of the effective range theory. We also show that, by including higher order corrections, one can obtain results that are close to those of the accurate potential model.

PACS: 25.10.+s, 25.30.Bf, 25.40.Lw

¹E-mail:sando@triumf.ca

²E-mail:hch@meson.skku.ac.kr

1. Introduction

Effective field theory (EFT) has proven to provide a useful tool for describing a wide class of meson-meson, meson-nucleon, and nucleon-nucleon (NN) processes with and without external probes in the low energy regime[1]. As for the NN processes, the 1S_0 and $^3S_1 - ^3D_1$ channels require special care because of the very large scattering length for the former and a shallow bound state (the deuteron) for the latter. Whereas EFT is based on the perturbative expansion of physical observables in terms of small external momenta, a non-perturbative treatment is required for the long scattering length or the bound state. Weinberg has suggested counting rules that allow us to handle these non-perturbative problems and derive the NN potential systematically [2]. The S -matrix is calculated from a wave function obtained by solving the Schrödinger equation with the potential calculated to a given order. This scheme has shown good accuracy and convergence with only a few leading terms [3, 4]. Kaplan, Savage, and Wise (KSW) suggested an alternative approach, the so-called power divergence subtraction (PDS) scheme, to the non-perturbative NN systems [5]. Treating only the leading order (LO) term non-perturbatively, KSW were able to obtain physical observables directly from the Feynman diagrams expanded order by order. Over the last decade both the Weinberg and PDS schemes have been used extensively in studying few-nucleon systems; for reviews see, *e.g.*, Refs. [6] and [7].

In the PDS scheme the convergence of the deuteron observables becomes slow due to a large expansion parameter $\gamma \rho_d \simeq 0.4$, where $\gamma \simeq 45.7$ MeV and $\rho_d \simeq 1.764$ fm, near the deuteron pole. It was suggested that adjusting the deuteron wave function to fit the asymptotic S -state normalization constant, $Z_d = \gamma \rho_d / (1 - \gamma \rho_d)$, assures more efficient convergence [8, 9, 10]. By introducing a dibaryon field which represents a resonance state (or a bound state) of two nucleons³, Beane and Savage showed that in terms of dibaryon EFT (dEFT), the long tail of the deuteron wave function can be naturally derived from the two-nucleon(dibaryon) propagator at the deuteron pole [12]. It was also shown that, with the use of dEFT, a good number of diagrams at a given order in the PDS scheme can be cast into a few diagrams. This feature is expected to be useful when higher order corrections need to be calculated. One can also expect that dEFT should be an attractive approach in attempts to incorporate, in the framework of EFT, radiative corrections (the photon degree of freedom) for the two-nucleon reactions [13, 14].

In applying dEFT to reactions with an external probe, there appear additional unknown low energy constants (LEC's) in the effective lagrangian. These LEC's are considered to subsume the high energy physics, such as meson exchange currents or heavy meson exchanges, that has been integrated out from the effective lagrangian. Since the values of these LEC's in general cannot be determined from symmetry, they need to be fixed either from experimental data or from direct calculations based on the underlying theory, QCD. For example, LEC's that enter into the electromagnetic (EM) interaction on the two-nucleon system can be fixed from the total cross section of radiative neutron

³Initially, the dibaryon field was introduced by Kaplan in the 1S_0 channel NN scattering [11]. It was shown that the pole structure of the amplitude at the low energies can be more efficiently reproduced with the use of the dibaryon field.

capture on a proton, $np \rightarrow d\gamma$, or from the deuteron EM multipole moments.⁴ Since each version of EFT has its own expansion scheme, the value of LEC's for a given vertex can differ from one version to another. However, in order to keep consistency with order counting, every EFT should satisfy a common requirement that the terms involving these LEC's should be minor corrections to the LO contributions.

In this work, we make extensive applications of dEFT to the deuteron reactions. We consider a pion-less effective lagrangian that includes the dibaryon fields in the 1S_0 and $^3S_1 - ^3D_1$ channels. The LEC's appearing in the strong interaction part of the dibaryon lagrangian are fixed by the effective range parameters in each channel. The EM interactions between the dibaryon fields and an external probe introduce additional LEC's in both isoscalar and isovector transitions. The LEC's for the vector(photon)-dibaryon-dibaryon (Vdd) vertices are fixed by experimental data in the conventional renormalization scheme. The contributions from them, however, turn out to be larger than those found in the conventional EFT's due to the factor $1/(1 - \gamma\rho_d)$, which arises from the normalization factor Z_d of the deuteron wave-function (or equivalently, from the asymptotic S -state normalization constant). We suppose that a prime portion of the LEC's of the Vdd vertices in dEFT originates mainly from the one-body vector(photon)-nucleon-nucleon (VNN) interactions so that this contribution together with that from the leading two-nucleon loop diagram cancels out the factor $1/(1 - \gamma\rho_d)$ in Z_d . We find that this scheme for fixing the LEC's well reproduces the deuteron EM form factors and the total cross section for $np \rightarrow d\gamma$ obtained in the effective range theory (ERT). Including higher order terms in our dEFT calculations, we find that the results of the dEFT become comparable to those of the potential model calculation.

The paper is organized as follows: In Sect. 2 the effective lagrangian is given. We calculate in Sect. 3 the EM form factors of the deuteron and fix the LEC's in the EM interaction lagrangians. We then calculate the physical observables in the elastic e - d scattering, and compare the results with those of ERT and a potential model calculation and also with the experimental data. In Sect. 4, we investigate the $np \rightarrow d\gamma$ reaction. The final section, Sect. 5, is devoted to discussion and conclusions. In Appendix, we give details on the two-nucleon(dibaryon) propagators and determine the LEC's in the strong-interaction lagrangian.

2. Effective lagrangian with dibaryon fields

A pionless effective lagrangian for the nucleon and the dibaryon fields interacting with an external vector field can be written as

$$\mathcal{L} = \mathcal{L}_N + \mathcal{L}_s + \mathcal{L}_t + \mathcal{L}_{st}, \quad (1)$$

where \mathcal{L}_N is the one-nucleon lagrangian, \mathcal{L}_s and \mathcal{L}_t are the lagrangians for the dibaryon fields in the 1S_0 and 3S_1 channels, respectively. \mathcal{L}_{st} is the lagrangian that accounts for the transition between 1S_0 and 3S_1 channels through the isovector EM interaction.

⁴Recently Detmold and Savage [15] suggested that lattice simulations allow us to estimate the LEC's that feature in dEFT describing reactions with an external probe.

\mathcal{L}_N in the heavy-baryon formalism reads

$$\mathcal{L}_N = N^\dagger \left\{ iv \cdot D + \frac{1}{2m_N} \left[(v \cdot D)^2 - D^2 - i[S^\mu, S^\nu] \left((1 + \kappa_V) f_{\mu\nu}^+ + (1 + \kappa_S) v_{\mu\nu}^S \right) \right] \right\} N, \quad (2)$$

where v^μ is the velocity vector satisfying $v^2 = 1$; we take $v^\mu = (1, \vec{0})$. S^μ is the spin operator $2S^\mu = (0, \vec{\sigma})$. $D_\mu = \partial_\mu - \frac{i}{2} \vec{\tau} \cdot \vec{v}_\mu - \frac{i}{2} v_\mu^S$, where \vec{v}_μ and v_μ^S are the external isovector and isoscalar vector currents, respectively. $f_{\mu\nu}^+ = \frac{i}{2} \cdot (\partial_\mu \vec{v}_\nu - \partial_\nu \vec{v}_\mu)$ and $v_{\mu\nu}^S = \frac{1}{2} (\partial_\mu v_\nu^S - \partial_\nu v_\mu^S)$. m_N is the nucleon mass and κ_V (κ_S) is the isovector (isoscalar) anomalous magnetic moment of the nucleon; $\kappa_V = 3.70589$ ($\kappa_S = -0.12019$).

\mathcal{L}_s , \mathcal{L}_t , and \mathcal{L}_{st} for the dibaryon fields read

$$\mathcal{L}_s = \sigma_s s_a^\dagger \left[iv \cdot D + \frac{1}{4m_N} [(v \cdot D)^2 - D^2] + \Delta_s \right] s_a - y_s \left[s_a^\dagger (N^T P_a^{(1S_0)} N) + \text{h.c.} \right], \quad (3)$$

$$\begin{aligned} \mathcal{L}_t = & \sigma_t t_i^\dagger \left[iv \cdot D + \frac{1}{4m_N} [(v \cdot D)^2 - D^2] + \Delta_t \right] t_i - y_t \left[t_i^\dagger (N^T P_i^{(3S_1)} N) + \text{h.c.} \right] \\ & - \frac{C_2^{(sd)}}{\sqrt{m_N \rho_d}} \mathcal{T}_{ij,xy}^{(sd)} \left[t_i^\dagger (N^T \mathcal{O}_{xy,j}^{(2)} N) + \text{h.c.} \right] - \frac{2L_2}{m_N \rho_d} i \epsilon_{ijk} t_i^\dagger t_j B_k \\ & - \frac{L'_2}{\sqrt{m_N \rho_d}} \left[i \epsilon_{ijk} t_i^\dagger \left(N^T P_j^{(3S_1)} N \right) B_k + \text{h.c.} \right] + \frac{2C_M}{m_N \rho_d} i \epsilon_{ijk} t_i^\dagger \{ D^2, B_j \} t_k \\ & - \frac{C_Q}{m_N \rho_d} t_i^\dagger \left[iv \cdot D, \mathcal{O}_{ij}^{(2)} \right] t_j, \end{aligned} \quad (4)$$

$$\begin{aligned} \mathcal{L}_{st} = & \frac{eL_1}{m_N \sqrt{r_0 \rho_d}} \left[t_i^\dagger s_3 B_i + \text{h.c.} \right] + \frac{L'_1}{\sqrt{m_N \rho_d}} \left[t_i^\dagger \left(N^T P_3^{(1S_0)} N \right) B_i + \text{h.c.} \right] \\ & + \frac{L'_1}{\sqrt{m_N r_0}} \left[\left(N^T P_i^{(3S_1)} N \right)^\dagger s_3 B_i + \text{h.c.} \right]. \end{aligned} \quad (5)$$

The covariant derivative for the dibaryon field is given by $D_\mu = \partial_\mu - iCv_\mu^{ext}$, where v_μ^{ext} is the external vector field and C is the charge operator of the dibaryon field. \vec{B} is the magnetic field given by $\vec{B} = \nabla \times \vec{v}^{ext}$. The sign factors, σ_s and σ_t , turn out to be -1 (see Appendix for details). Δ_t (Δ_s) is the difference between the dibaryon mass m_t (m_s) in the 3S_1 (1S_0) channel and the two-nucleon mass $m_{t,s} = 2m_N + \Delta_{t,s}$. ρ_d and r_0 are the effective ranges for the deuteron and 1S_0 scattering state, respectively. $P_i^{(S)}$ is the projection operator for the $S = {}^3S_1$ or 1S_0 channel;

$$P_i^{(3S_1)} = \frac{1}{\sqrt{8}} \sigma_2 \sigma_i \tau_2, \quad P_a^{(1S_0)} = \frac{1}{\sqrt{8}} \sigma_2 \tau_2 \tau_a, \quad \text{Tr}(P_i^{(S)\dagger} P_j^{(S)}) = \frac{1}{2} \delta_{ij}, \quad (6)$$

where σ_i (τ_a) is the spin (isospin) operator. The operators for the D -state read

$$\mathcal{T}_{ij,xy}^{(sd)} = \delta_{ix} \delta_{jy} - \frac{1}{3} \delta_{ij} \delta_{xy}, \quad \mathcal{O}_{ij}^{(2)} = - \left(\nabla_i \nabla_j - \frac{1}{3} \delta_{ij} \nabla^2 \right), \quad (7)$$

$$\mathcal{O}_{xy,j}^{(2)} = -\frac{1}{4} \left(\overleftarrow{D}_x \overleftarrow{D}_y P_j^{(3S_1)} + P_j^{(3S_1)} \overrightarrow{D}_x \overrightarrow{D}_y - \overleftarrow{D}_x P_j^{(3S_1)} \overrightarrow{D}_y - \overleftarrow{D}_y P_j^{(3S_1)} \overrightarrow{D}_x \right). \quad (8)$$

The LEC's, y_s and y_t , represent the dibaryon- NN (dNN) couplings in the spin singlet and triple states, respectively, and they contribute to the two-nucleon loop diagram for the two-nucleon(dibaryon) propagator. They, as well as $\Delta_{s,t}$ and $\sigma_{s,t}$, have been determined from the effective ranges in the 1S_0 scattering and the deuteron states. $C_2^{(sd)}$ accounts for 3D_1 state mixture to the 3S_1 state and is fixed by the asymptotic D - S ratio η_{sd} ($\simeq 0.0254$). Details are given in the Appendix.

C_Q , C_M , L_1 , and L_2 are the LEC's for the Vdd vertices, and L'_1 and L'_2 for the vector(photon)-dibaryon- NN ($VdNN$) vertices. C_Q is determined from the electric quadrupole moment of the deuteron, while L_1 (L'_1) and L_2 (L'_2) are determined from the total cross section of the radiative neutron capture by the proton and the magnetic moment of the deuteron, respectively. In this work we introduce a new LEC C_M , which can be fixed from the radius of the magnetic form factor of the deuteron. In the next two sections, we determine the EM LEC's listed above and proceed to calculate the EM observables in the elastic e - d scattering.

3. EM form factors of the deuteron

The EM form factors of the deuteron have been intensively studied within Weinberg's approach [9, 16] as well as in the PDS scheme with and without pions [17, 18]. The electric form factor of the deuteron has also been calculated in dEFT without pions [12]. In this section we consider the deuteron EM form factors in dEFT without pions.

A deuteron state $|\vec{p}, i\rangle$ specified by momentum \vec{p} and spin i satisfies the normalization condition $\langle \vec{p}', i | \vec{p}, j \rangle = (2\pi)^3 \delta^{(3)}(\vec{p}' - \vec{p}) \delta_{ij}$. The nonrelativistic expansion of the matrix element of the electromagnetic current up to next-to-next-leading order (NNLO) is given as [18]

$$\begin{aligned} \langle \vec{p}', i | J_{em}^0 | \vec{p}, j \rangle &= e \left[F_C(q) \delta_{ij} + \frac{1}{2m_d^2} F_Q(q) \left(q_i q_j - \frac{1}{n-1} q^2 \delta_{ij} \right) \right] \left(\frac{E' + E}{2m_d} \right), \\ \langle \vec{p}', i | J_{em}^k | \vec{p}, j \rangle &= \frac{e}{2m_d} \left[F_C(q) \delta_{ij} (\vec{p}' + \vec{p})^k + F_M(q) (\delta_i^k q_j - \delta_j^k q_i) \right. \\ &\quad \left. + \frac{1}{2m_d^2} F_Q(q) \left(q_i q_j - \frac{1}{n-1} q^2 \delta_{ij} \right) (\vec{p}' + \vec{p})^k \right], \end{aligned} \quad (9)$$

where $\vec{p}' = \vec{p} + \vec{q}$ and $q = |\vec{q}|$. e is the electric charge, m_d the deuteron mass, and E (E') the energy of the deuteron in the initial (final) state. n is the space-time dimension, $n = 4$. The dimensionless form factors defined in Eq. (9) are conventionally normalized as

$$F_C(0) = 1, \quad \frac{e}{2m_d} F_M(0) = \mu_M, \quad \frac{1}{m_d^2} F_Q(0) = \mu_Q, \quad (10)$$

where $\mu_M = 0.85741 \frac{e}{2m_N} (\equiv \mu_d \frac{e}{2m_N})$ is the magnetic moment of the deuteron and $\mu_Q = 0.2859 \text{ fm}^2$ is its electric quadrupole moment. The charge radius of the deuteron $\sqrt{\langle r_{ch}^2 \rangle}$ is defined by $F_C(q) = 1 - \frac{1}{6} \langle r_{ch}^2 \rangle q^2 + \dots$ and its empirical value is $\sqrt{\langle r_{ch}^2 \rangle} = 2.1303 \text{ fm}$.

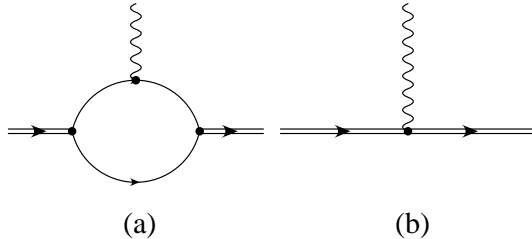


Figure 1: Diagrams for the deuteron electric form factor. The single line stands for the nucleon field, the double line for the dibaryon, and the wavy line for the photon. Both diagrams belong to $\mathcal{O}(Q^0)$.

3.1 Electric form factor

For the electric form factor of the deuteron, there are two LO, $\mathcal{O}(Q^0)$, diagrams, which are shown in Fig. 1. The three-point vertices in Figs. 1 (a) and (b) are given by

$$i\Gamma_{(ij)}^{(a)\mu} = -i\delta_{ij}v^\mu\sigma_t \frac{4}{\rho_d q} \arctan\left(\frac{q}{4\gamma}\right), \quad (11)$$

$$i\Gamma_{(ij)}^{(b)\mu} = i\delta_{ij}v^\mu\sigma_t, \quad (12)$$

where i and j denote the final and the initial spin state of the deuteron, respectively; μ is the Lorenz index for the current. Multiplying the three-point vertices with the normalization factor Z_d of the deuteron wave function, one obtains the charge form factor of the deuteron at LO as

$$v^\mu F_C^{LO}(q)\delta_{ij} = Z_d \left[\Gamma_{(ij)}^{(a)\mu} + \Gamma_{(ij)}^{(b)\mu} \right], \quad (13)$$

with

$$F_C^{LO}(q) = \frac{\rho_d \gamma}{1 - \rho_d \gamma} \left[\frac{4}{\rho_d q} \arctan\left(\frac{q}{4\gamma}\right) - 1 \right]. \quad (14)$$

This result is equivalent to that of the ERT [17] and gives the same charge radius $\langle r_{ch}^2 \rangle$ as ERT, $\langle r_{ch}^2 \rangle^{ER} = \frac{1}{8\gamma^2} \frac{1}{1 - \gamma\rho_d} = (1.985)^2$ fm 2 . Higher order corrections of $\mathcal{O}(Q^2)$ to $F_C(q)$ were studied in Ref. [18], in which it was shown that the main correction comes from the isoscalar vector radius of the nucleon current.

One can easily verify that Eq. (14) satisfies the normalization condition given by Eq. (10). It would be worth noting that the expression of $F_C(q)$ in Eq. (14) has no free parameter because the leading Vdd vertex that contributes to the electric form factor stems from the covariant derivative of the dibaryon field (Fig. 1 (b)), which is proportional to the dibaryon charge C and the overall factor σ_t . At $q = 0$, the contribution of the diagram with Vdd vertex (Fig. 1 (b)) amounts to -40% of that with the VNN vertex (Fig. 1 (a)). As will be shown in the next subsections, we find similar values of the Vdd

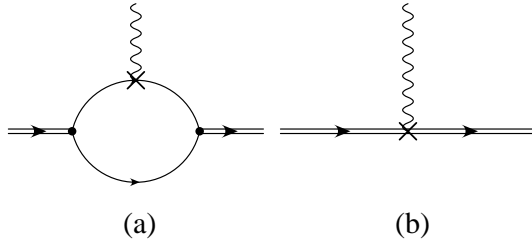


Figure 2: Diagrams contributing to the deuteron magnetic form factor. The leading order diagram (a) is $\mathcal{O}(Q)$, while the next-to-leading order diagram (b) is *formally* $\mathcal{O}(Q^2)$. The vertex with “X” in (a) is proportional to $(1 + \kappa_S)/(2m_N)$ while that with “X” in (b) is proportional to L_2 .

to VNN ratios for the other form factors. More importantly, the quantity in the bracket of Eq. (14) exactly cancels the factor $1/(1 - \gamma\rho_d)$ in the deuteron normalization factor at $q = 0$, which leads us to assign a new role to the LEC’s of the Vdd vertices.

3.2 Magnetic form factor

Diagrams contributing to the magnetic form factor of the deuteron are depicted in Fig. 2. The order of Fig. 2 (a) is LO ($\mathcal{O}(Q)$) and that of Fig. 2 (b) is *formally* next-to-leading order (NLO) ($\mathcal{O}(Q^2)$) for the vertex functions. We will discuss however that the contribution of Fig. 2 (b) can be separated into LO and sub-leading parts, and show that this re-ordering satisfies the order counting fairly well. The three-point vertex for each diagram is

$$i\Gamma_{(ij)k}^{(a)} = i(\delta_{ik}q_j - \delta_{jk}q_i) \frac{1 + \kappa_S}{2m_N} \frac{4}{\rho_d q} \arctan\left(\frac{q}{4\gamma}\right), \quad (15)$$

$$i\Gamma_{(ij)k}^{(b)} = i(\delta_{ik}q_j - \delta_{jk}q_i) \frac{2eL_2}{m_N \rho_d}, \quad (16)$$

where k is the index for the spacial part of the vector current. Multiplying the three-point functions with the normalization factor Z_d , one has the magnetic form factor $F_M(q)$,

$$\frac{1}{2m_d} F_M(q) = \frac{\gamma\rho_d}{1 - \gamma\rho_d} \left[\frac{1 + \kappa_S}{2m_N} \frac{4}{\rho_d q} \arctan\left(\frac{q}{4\gamma}\right) + \frac{2L_2}{m_N \rho_d} \right]. \quad (17)$$

At $q = 0$,

$$\frac{1}{2m_d} F_M(0) = \frac{\gamma\rho_d}{1 - \gamma\rho_d} \left[\frac{1 + \kappa_S}{2m_N} \frac{1}{\gamma\rho_d} + \frac{2L_2}{m_N \rho_d} \right]. \quad (18)$$

If one fixes the LEC L_2 using the experimental value of the deuteron magnetic moment μ_M in Eq. (10), one obtains $L_2 = -0.4033$ fm. Comparing the magnitude of Fig. 2 (a) with that of Fig. 2 (b), one finds that the latter is about -42% of the former, which is

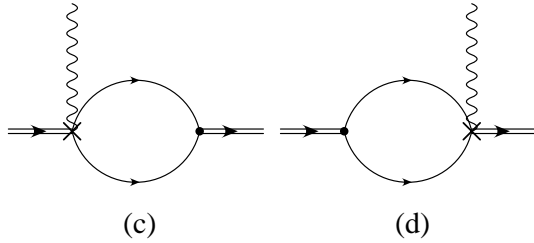


Figure 3: $\mathcal{O}(Q^3)$ contributions to the deuteron magnetic form factor arising from the L'_2 term. The “X” in the diagrams denotes the $VdNN$ vertex corresponding to L'_2 .

similar to the Vdd to VNN ratio for $F_C(0)$. Since this rather large ratio makes it difficult to regard the contribution of L_2 as the high energy contribution, we divide L_2 into the sum of the LO and sub-leading contributions.⁵ Thus

$$L_2 = L_2^0 + \delta L_2, \quad L_2^0 = -\frac{1}{4}(1 + \kappa_S)\rho_d, \quad (19)$$

where L_2^0 is LO, while δL_2 accounts for the sub-leading contributions. Inserting L_2^0 into L_2 of the lagrangian, one finds that the coefficient of the Vdd interaction becomes $(1 + \kappa_S)/(2m_N)$ which is the same as that of the one-body interaction. Note that L_2^0 is of Q^{-1} because of the factor ρ_d , so the diagram Fig. 2 (b) becomes the same order as the diagram Fig. 2 (a). The magnetic form factor at LO becomes

$$\begin{aligned} \frac{1}{2m_d} F_M(q) \Big|_{L_2=L_2^0} &= \frac{1 + \kappa_S}{2m_N} \frac{\gamma\rho_d}{1 - \gamma\rho_d} \left[\frac{4}{\rho_d q} \arctan\left(\frac{q}{4\gamma}\right) - 1 \right] \\ &= \frac{1 + \kappa_S}{2m_N} F_C^{LO}(q), \end{aligned} \quad (20)$$

which is equivalent to the relation of ERT[17]. Numerically, one finds $L_2^0 \simeq -0.3880$ fm. This value is larger than L_2 fixed from Eq. (10) by about 3.7 %, which can be attributed to the contribution of δL_2 .

Next we consider the contributions of NNLO, $\mathcal{O}(Q^3)$, from L'_2 of the $VdNN$ vertex (Fig. 3) and the D -wave of the deuteron (Fig. 4). Since there are no corrections to the isoscalar magnetic VNN vertex from the third order heavy-baryon chiral lagrangian [20], we do not have NLO corrections to $F_M(q)$ from the one-body sector.⁶ From the diagrams in Fig. 3 one obtains a three-point vertex function

$$i\Gamma_{(ij)k}^{(c+d)} = i(\delta_{ik}q_j - \delta_{jk}q_i) \frac{2\gamma}{m_N\rho_d} \sqrt{\frac{m_N}{2\pi}} L'_2, \quad (21)$$

⁵The same partition has been employed for the LEC L_2 in the recent dEFT calculations[15, 19].

⁶At NNLO, there are additional corrections from the radius and relativistic corrections to the isoscalar magnetic nucleon current. Since we are interested here in the role of LEC’s in the two-nucleon(dibaryon) sector, we skip those additional contributions; we will include them in a later subsection where the elastic e - d scattering is considered.

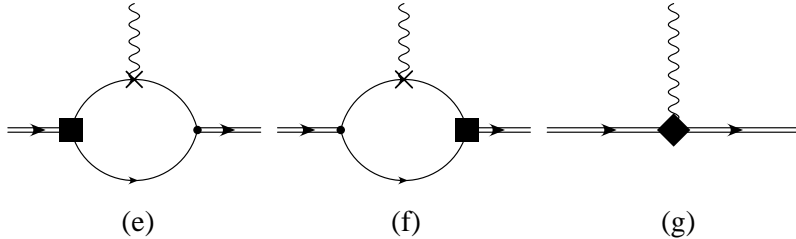


Figure 4: $\mathcal{O}(Q^3)$ contributions to the deuteron magnetic form factor arising from the deuteron D -wave. The “X” denotes the isoscalar magnetic vertex of nucleon-photon coupling proportional to $(1 + \kappa_S)/(2m_N)$, and the filled boxes stand for the deuteron D -wave in the diagrams (e) and (f). The filled diamond in the diagram (g) is a vertex proportional to C_M .

where dimensional regularization has been used for the loop integration. The sum of the diagrams in Fig. 4 gives

$$\begin{aligned} i\Gamma_{(ij)k}^{(e+f)} &= i(\delta_{ik}q_j - \delta_{jk}q_i) \frac{\sqrt{2}(1 + \kappa_S)\eta_{sd}}{32m_N\rho_d\gamma^2q} \left[4\gamma q - (16\gamma^2 + 3q^2)\arctan\left(\frac{q}{4\gamma}\right) \right], \\ i\Gamma_{(ij)k}^{(g)} &= i(\delta_{ik}q_j - \delta_{jk}q_i) \frac{2C_M}{m_N\rho_d} (\vec{p'}^2 + \vec{p}^2). \end{aligned} \quad (22)$$

Summing up the contributions from Fig. 2 to Fig. 4, we obtain the magnetic form factor of the deuteron up to NNLO as

$$\begin{aligned} \frac{1}{2m_d}F_M(q) &= \frac{\gamma\rho_d}{1 - \gamma\rho_d} \left\{ \frac{1 + \kappa_S}{2m_N} \left[\frac{4}{\rho_d q} \arctan\left(\frac{q}{4\gamma}\right) - 1 \right. \right. \\ &\quad \left. \left. + \frac{\sqrt{2}\eta_{sd}}{16\gamma^2\rho_d q} \left(4\gamma q - (16\gamma^2 + 3q^2)\arctan\left(\frac{q}{4\gamma}\right) \right) \right] \right. \\ &\quad \left. + \frac{2\gamma}{m_N\rho_d} \sqrt{\frac{m_N}{2\pi}} L'_2 + \frac{2C_M}{m_N\rho_d} (\vec{p'}^2 + \vec{p}^2) \right\}, \end{aligned} \quad (23)$$

where we have put $L_2 = L_2^0$. Fixing L'_2 from Eq. (10), we obtain $L'_2 = -0.07096 \text{ fm}^{5/2}$. We will study below the role of higher order corrections to the $F_M(q)$ form factor in elastic e - d scattering.

3.3 Electric quadrupole form factor

Diagrams for the electric quadrupole form factor of the deuteron are depicted in Fig. 5. The diagrams (a) and (b) are $\mathcal{O}(Q^2)$, while the diagram (c) is *formally* one order higher, $\mathcal{O}(Q^3)$. As before, however, it turns out that this formal counting fails for dEFT. We will show below that the same assumption as used for the LEC L_2 in Eq. (19) can be used here to extract the LO part of C_Q .

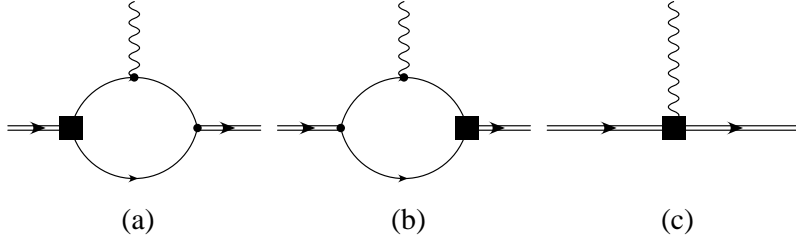


Figure 5: Diagrams for the electric quadrupole form factor of the deuteron. The order of the (a,b) diagrams is of Q^2 and that of the (c) diagram is *formally* of Q^3 . The filled boxes in the (a,b) diagrams denote the D -wave contribution and that in the (c) diagram represents a vertex proportional to C_Q .

Three-point vertex functions from the diagrams in Fig. 5 are obtained as

$$i\Gamma_{(ij)}^{(a+b)\mu} = iv^\mu \left(q_i q_j - \frac{1}{3} \delta_{ij} q^2 \right) \frac{3}{4\sqrt{2}} \frac{\eta_{sd}}{\rho_d \gamma^2 q^3} \left[-4\gamma q + (16\gamma^2 + 3q^2) \arctan \left(\frac{q}{4\gamma} \right) \right], \quad (24)$$

$$i\Gamma_{(ij)}^{(c)\mu} = iv^\mu \left(q_i q_j - \frac{1}{3} q^2 \delta_{ij} \right) \frac{C_Q}{m_N \rho_d}. \quad (25)$$

Multiplying the three-point functions with the factor Z_d , we obtain

$$\frac{F_Q(q)}{2m_d^2} = \frac{\rho_d \gamma}{1 - \rho_d \gamma} \left\{ \frac{3}{4\sqrt{2}} \frac{\eta_{sd}}{\rho_d \gamma^2 q^3} \left[-4\gamma q + (16\gamma^2 + 3q^2) \arctan \left(\frac{q}{4\gamma} \right) \right] + \frac{C_Q}{m_N \rho_d} \right\}, \quad (26)$$

and at $q = 0$

$$\frac{F_Q(0)}{m_d^2} = \frac{2\rho_d \gamma}{1 - \rho_d \gamma} \left[\frac{1}{2\sqrt{2}} \frac{\eta_{sd}}{\rho_d \gamma^3} + \frac{C_Q}{m_N \rho_d} \right]. \quad (27)$$

The normalization condition Eq. (10), leads to $C_Q = -1.709$ fm 2 . Comparing the first and second terms in the bracket in Eq. (27), one finds that the latter is about -50% of the former and the C_Q term is much larger than the estimations in the previous EFT calculations. In addition, it shows a pattern similar to what we have already seen in the cases of $F_C(q)$ and $F_M(q)$. Now we assume that the prime portion of the LEC C_Q in dEFT, denoted by C_Q^0 , should make the factor $(1 - \rho_d \gamma)$ together with the contributions from the two-nucleon loop diagrams (Fig. 5 (a) and (b)) in order to kill the factor $(1 - \rho_d \gamma)^{-1}$ in Z_d ; this way $F_Q(q)$ at $q = 0$ becomes a normal size, and the remainder, δC_Q , accounts for the contribution of the high energy physics. Thus we have

$$C_Q = C_Q^0 + \delta C_Q, \quad C_Q^0 = -\frac{1}{2\sqrt{2}} \frac{\eta_{sd}}{\gamma^2} m_N \rho_d, \quad (28)$$

where numerically $C_Q^0 = -1.408$ fm 2 . The contribution of δC_Q to μ_Q is about -17.2% . This rearrangement of C_Q leads to reconciliation between dEFT and the former EFT calculations.

3.4 Elastic electron-deuteron scattering

With the use of the deuteron form factors obtained above we now make a brief study of elastic electron-deuteron scattering, $e + d \rightarrow e + d$. The differential cross section of the reaction is given by

$$\frac{d\sigma}{d\Omega} = \left. \frac{d\sigma}{d\Omega} \right|_{Mott} \left[A(q) + B(q) \tan^2 \left(\frac{\theta}{2} \right) \right]. \quad (29)$$

The form factors $A(q)$ and $B(q)$ here are related to the deuteron form factors via

$$A(q) = F_C^2(q) + \frac{2}{3}\eta F_M^2(q) + \frac{8}{9}\eta^2 F_Q^2(q), \quad B(q) = \frac{4}{3}\eta(1+\eta)F_M^2(q), \quad (30)$$

with $\eta = q^2/(4m_d^2)$.

To incorporate other NNLO corrections which have not been considered explicitly in the previous subsections, we introduce the radius of the isoscalar vector nucleon current and a radius correction from the dibaryon field to the electric form factor $F_C(q)$. Thus we write

$$F_C(q) = \frac{\rho_d \gamma}{1 - \rho_d \gamma} \left\{ \left[\frac{4}{\rho_d q} \arctan \left(\frac{q}{4\gamma} \right) - 1 \right] \left(1 - \frac{1}{6} \langle r_{Es}^2 \rangle q^2 \right) - \frac{1}{6} \delta_c q^2 \right\}, \quad (31)$$

where $\langle r_{Es}^2 \rangle$ is the isoscalar-electric radius of the nucleon Sachs form factor,⁷ $\langle r_{Es}^2 \rangle = 0.604$ fm², and δ_c is a subleading radius correction from the dibaryon field. The corrected charge radius reads $\langle r_{ch}^2 \rangle = \frac{1}{1 - \rho_d \gamma} \frac{1}{8\gamma^2} + \langle r_{Es}^2 \rangle + Z_d \delta_c$. Using the experimental value of $\langle r_{ch}^2 \rangle$, we obtain $\delta_c = -0.011$ fm². Similarly, the introduction of the nucleon radius in the $F_M(q)$ leads to

$$\begin{aligned} \frac{e}{2m_d} F_M(q) = & \frac{e\gamma\rho_d}{1 - \gamma\rho_d} \left\{ \frac{1 + \kappa_S}{2m_N} \left(1 - \frac{1}{6} \langle r_{Ms}^2 \rangle q^2 \right) \left[\frac{4}{\rho_d q} \arctan \left(\frac{q}{4\gamma} \right) - 1 \right. \right. \\ & \left. \left. + \frac{\sqrt{2}\eta_{sd}}{16\gamma^2\rho_d q} \left(4\gamma q - (16\gamma^2 + 3q^2) \arctan \left(\frac{q}{4\gamma} \right) \right) \right] \right. \\ & \left. + \frac{2\gamma}{m_N\rho_d} \sqrt{\frac{m_N}{2\pi}} L'_2 + \frac{2\delta C_M}{m_N\rho_d} q^2 \right\}, \end{aligned} \quad (32)$$

where we have separated the LEC $C_M = C_M^0 + \delta C_M$ and fixed the value of C_M^0 by the one-body radius, isoscalar-magnetic radius of the Sachs form factor of the nucleon, $\langle r_{Ms}^2 \rangle = 0.598$ fm². LEC δC_M can be fixed from the radius $\sqrt{\langle r_{Md}^2 \rangle}$ of $F_M(q)$. From Eq. (32) one obtains the relation for $\langle r_{Md}^2 \rangle$,

$$\langle r_{Md}^2 \rangle = \frac{e}{\mu_M} \left\{ \frac{1 + \kappa_S}{2m_N} \left[\frac{1 + \sqrt{8}\eta_{sd}}{(1 - \gamma\rho_d)8\gamma^2} + \langle r_{Ms}^2 \rangle \right] - \frac{12\gamma\delta C_M}{(1 - \gamma\rho_d)m_N} \right\}. \quad (33)$$

⁷We have obtained the values of the nucleon radii $\langle r_{Es}^2 \rangle$ and $\langle r_{Ms}^2 \rangle$ from $r_1^{(s)}$ and $r_2^{(s)}$, the isoscalar radii for the Dirac and Pauli form factors, given in Table 1 of Ref. [21].

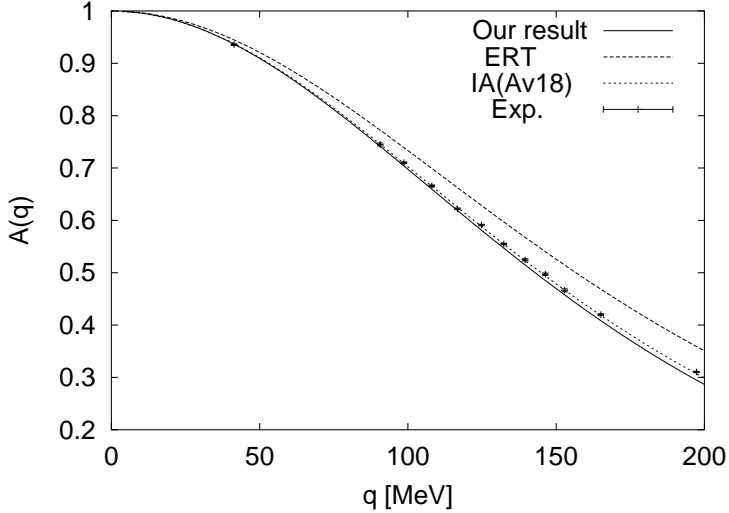


Figure 6: Form factor $A(q)$ in the elastic e - d scattering. The solid line corresponds to our present result, the dashed line to the result of ERT, and the dotted line to that of the accurate potential model calculation that includes the one-body (IA) operator [22]. The experimental data are taken from Ref. [23].

Unfortunately, precise experimental data of $\langle r_{Md}^2 \rangle$ are not available yet. So we adjust δC_M by fitting it to the elastic e - d scattering data up to the momentum transfer $q = 400$ MeV. Here we adopt $\sqrt{\langle r_{Md}^2 \rangle} = 2.135$ fm to fix the value of δC_M . We ignore the radius effects in $F_Q(q)$ because the contribution of $F_Q(q)$ to $A(q)$ is negligible in the momentum range under consideration.

The results for $A(q)$ and $B(q)$ are shown in Figs. 6 and 7, respectively. In both figures, the solid lines represent our present results, the dashed lines correspond to the results of ERT, and the dotted lines to those of a potential model calculation which we evaluated by using the Argonne v18 potential (Av18) and the one-body (IA) operator [22]. The experimental data in Fig. 6 are taken from Ref. [23]. Our LO dEFT calculations reproduce well the results of ERT in the small momentum region. With the higher order corrections included, the results of the dEFT approach improve those of ERT and give results comparable to those of the accurate potential model calculations for both $A(q)$ and $B(q)$ at large momenta. It is to be remarked that, in dEFT, we use the empirical values of r_{ch} and μ_d and adjust r_{Md} to fix the LEC's, whereas ERT and the potential model calculation do not quite reproduce the empirical values of these observables; see Tab. 1. We should note that the experimental value of r_{Md} still has relatively large uncertainties. Since our result for $B(q)$ is sensitive to the value of r_{Md} , a more accurate measurement of r_{Md} is required to reduce the theoretical uncertainty in $B(q)$.

4. Radiative neutron capture by the proton

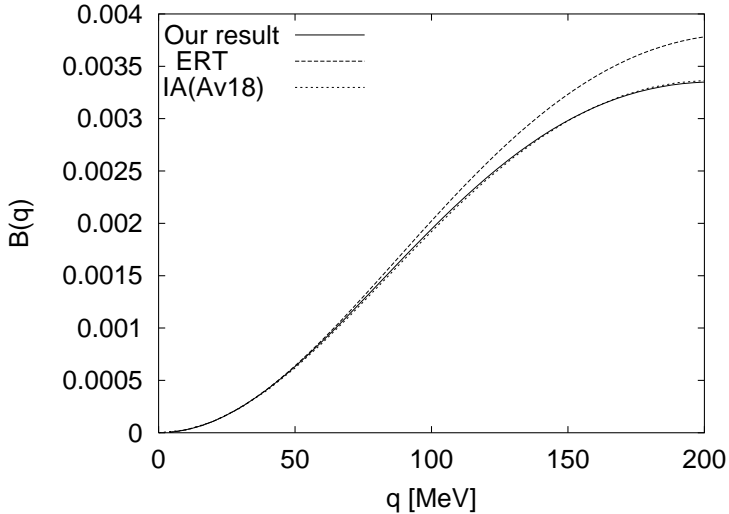


Figure 7: Form factor $B(q)$ in the elastic e - d scattering. For further explanations, see the caption for Fig. 6.

	ERT	IA(Av18)	dEFT	Exp.
r_{ch}	1.985	2.115	2.130*	2.130
r_{Md}	1.985	2.090	2.135*	—
μ_d	0.880	0.847	0.857*	0.857

Table 1: Comparison of the physical observables; radii, r_{ch} and r_{Md} , of the electric and magnetic form factors and the magnetic moment μ_d of the deuteron. r_{ch} and r_{Md} are given in units of fm. In the column representing dEFT, the entries with '*' are input used for fixing the LEC's.

Radiative neutron capture by the proton, $n + p \rightarrow d + \gamma$, has been intensively studied within the frameworks of EFT employing the Weinberg's scheme [24] and the PDS scheme with pions [25] and without pions [18]; see also [12]. We propose ourselves to study this reaction in more detail here.

Leading order, $\mathcal{O}(Q^{1/2})$, diagrams for the process are depicted in Fig. 8. The diagram (c) is *formally* $\mathcal{O}(Q^{3/2})$, thus of a higher order. However, we will discuss below that, because of the Vdd vertex involved, it is more appropriate to assign to diagram (c) the same order as diagrams (a) and (b). Summing up the contributions of diagrams (a), (b) and (c) in Fig. 8, one obtains the amplitudes for the initial 3S_1 and 1S_0 states as

$$i\mathcal{A}^{(a+b+c)}(^3S_1) = -i(\vec{\epsilon}_{(d)}^* \times \vec{\epsilon}_i) \cdot (\vec{\epsilon}_{(\gamma)}^* \times \hat{k}) \sqrt{\frac{2\pi\gamma}{1-\gamma\rho_d}} \frac{2}{m_N} \frac{1}{-\gamma - ip + \frac{1}{2}\rho_d(\gamma^2 + p^2)}$$

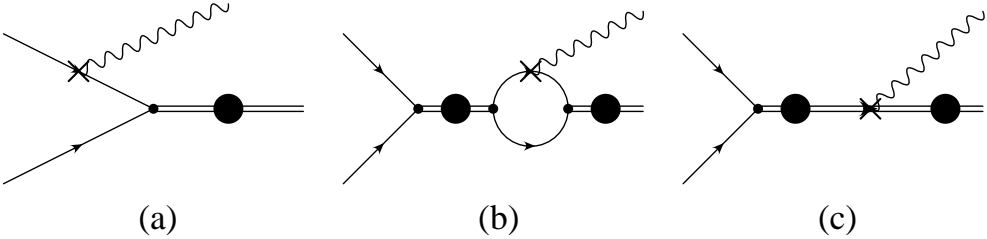


Figure 8: Diagrams contributing to $np \rightarrow d\gamma$: Diagrams (a) and (b) are $\mathcal{O}(Q^{1/2})$, while diagram (c) is *formally* $\mathcal{O}(Q^{3/2})$. The single lines, the double lines with a filled circle, and the wavy lines denote nucleons, dibaryons, and photons, respectively. See Appendix for more details.

$$\times \left[\frac{1 + \kappa_S}{2m_N} \frac{1}{2} \rho_d(\gamma^2 + p^2) + \frac{\gamma^2 + p^2}{m_N} L_2 \right], \quad (34)$$

$$\begin{aligned} i\mathcal{A}^{(a+b+c)}(^1S_0) = & \bar{\epsilon}_{(d)}^* \cdot (\hat{k} \times \bar{\epsilon}_{(\gamma)}^*) \sqrt{\frac{2\pi\gamma}{1 - \gamma\rho_d}} \frac{2}{m_N - \frac{1}{a_0} - ip + \frac{1}{2}r_0p^2} \\ & \times \left[\frac{1 + \kappa_V}{2m_N} \left(\gamma - \frac{1}{a_0} + \frac{1}{2}r_0p^2 \right) + \frac{\gamma^2 + p^2}{2m_N} L_1 \right]. \end{aligned} \quad (35)$$

Here \vec{p} is the relative momentum of the two-nucleon system, and \vec{k} is the momentum of the out-going photon; $p = |\vec{p}|$, $k = |\vec{k}|$, and $\hat{k} = \vec{k}/k$. $\bar{\epsilon}_{(d)}^*$ and $\bar{\epsilon}_{(\gamma)}^*$ are the polarization vectors for the out-going deuteron and photon, respectively, and $\vec{\epsilon}_i$ is the spin $S = 1$ vector for the initial 3S_1 state. a_0 and r_0 are, respectively, the scattering length and effective range of the neutron–proton 1S_0 state. The LEC L_2 has already been fixed in the previous section using the deuteron magnetic moment μ_M . The LEC L_1 should be fixed using some experimental information.

It is worth noting that the LO ($\mathcal{O}(Q^{1/2})$) amplitude for the 3S_1 state in Eq. (34) vanishes,

$$\mathcal{A}^{(a+b+c)}(^3S_1) \Big|_{L_2=L_2^0} = 0. \quad (36)$$

The expression of L_2^0 is given in Eq. (19). It is well known that the isoscalar transition between the scattering and bound states vanishes due to the orthogonality of the wave functions, and we confirm that our treatment of the LEC L_2^0 satisfies this condition. Although higher-order terms give non-vanishing contributions, δL_2 , δL_2 is found to be very small compared with the leading isovector amplitude; we therefore neglect the isoscalar part in our subsequent discussion.

We determine the value of L_1 in Eq. (35) from the cross section of $np \rightarrow d\gamma$ at the thermal energy, $\sigma^{exp} = 334.2 \pm 0.5$ mb [26]. The total cross section in the CM frame reads

$$\sigma = \frac{\alpha(\gamma^2 + p^2)}{4p} \sum_{spin} |\mathcal{A}|^2, \quad (37)$$

where α is the fine structure constant, and the CM energy E corresponding to the thermal neutron experiment is $E = p^2/m_N = 1.264 \times 10^{-8}$ MeV. Using the formula for the spin summation $\sum_{\text{spin}} |i\bar{\epsilon}_{(d)}^* \cdot (\hat{k} \times \bar{\epsilon}_{(\gamma)}^*)|^2 = 2$ and including only the amplitude for the 1S_0 channel, $\mathcal{A}(^1S_0)$ in Eq. (35), we obtain $L_1 = -4.427$ fm.

It is to be noted that, if L_1 is set equal to zero, *i.e.*, $L_1 = 0$, the relevant cross section would become $\sigma(L_1 = 0) = 502.3$ mb, which is about 1.5 times larger than the experimental value, *i.e.*, $\sigma(L_1 = 0)/\sigma^{\text{exp}} \simeq 1.50$. Meanwhile, the magnitude of the LO cross section in the PDS scheme is smaller than σ^{exp} by about 13 % [25]. Furthermore, the leading one-body operators in the potential model calculations also lead to a cross section that is smaller than σ^{exp} by about 10 %; as is well known, most of this 10 % deficiency can be accounted for by the meson exchange currents. Thus, here again we are facing the situation that, whereas the conventional treatments indicate the dominance of the LO contributions, the dEFT results exhibit uncomfortably large higher order corrections. To solve this problem, we assume that L_1 is dominated by a leading contribution denoted by L_1^0 which is chosen so as to reproduce the result of ERT, and that the rest, δL_1 contains information about the high energy physics that has been integrated out. Thus we consider the decomposition

$$L_1 = L_1^0 + \delta L_1, \quad L_1^0 = -\frac{1}{4}(1 + \kappa_V)(r_0 + \rho_d), \quad (38)$$

where numerically $L_1^0 = -5.275$ fm. If we insert the expression for L_1^0 into L_1 in the lagrangian, the coefficient of the Vdd term becomes $-\frac{1+\kappa_V}{2m_N} \frac{r_0+\rho_d}{2\sqrt{r_0\rho_d}}$, which is the coefficient of the one-body VNN interaction apart from a factor (which is very close to unity), $(r_0 + \rho_d)/(2\sqrt{r_0\rho_d}) \simeq 1.024$. With the assumption stated above, L_1^0 becomes $\mathcal{O}(Q^{-1})$ owing to the factor $(r_0 + \rho_d)$. Therefore, with the use of L_1^0 , the order of diagram (c) in Fig. 8 becomes the same as that of diagrams (a) and (b). At LO, the total cross section reads

$$\sigma(L_1^0) = \frac{\pi\alpha(1 + \kappa_V)^2\gamma^5a_0^2}{pm_N^4(1 - \gamma\rho_d)} \left[1 - \frac{1}{\gamma a_0} - \frac{\gamma}{4}(r_0 + \rho_d) \right]^2, \quad (39)$$

which is the same expression as that of ERT. Numerically we have $\sigma(L_1^0) = 304.9$ mb. This value is close to $\sigma_{IA} = 304.5$ mb obtained in the potential model with the use of the one-body operator.

Now we study higher order corrections for the $np \rightarrow d\gamma$ reaction. Higher order diagrams ($\mathcal{O}(Q^{5/2})$) with the $VdNN$ vertex proportional to L'_1 are depicted in Fig. 9. Note that the diagrams with the D -wave contribution vanish for the initial S -wave states and the corrections from the radii are negligible because of the tiny momentum transfer in the reaction. The combined contributions of diagrams (d,e,f) in Fig. 9 are given by

$$\begin{aligned} i\mathcal{A}^{(d+e+f)}(^1S_0) &= \bar{\epsilon}_{(d)}^* \cdot (\hat{k} \times \bar{\epsilon}_{(\gamma)}^*) \sqrt{\frac{2\pi\gamma}{1 - \gamma\rho_d}} \frac{2}{m_N - \frac{1}{a_0} - ip + \frac{1}{2}r_0p^2} \\ &\quad \times \frac{\gamma^2 + p^2}{2m_N} \sqrt{\frac{m_N}{2\pi}} \left(\gamma + \frac{1}{a_0} - \frac{1}{2}r_0p^2 \right) L'_1. \end{aligned} \quad (40)$$

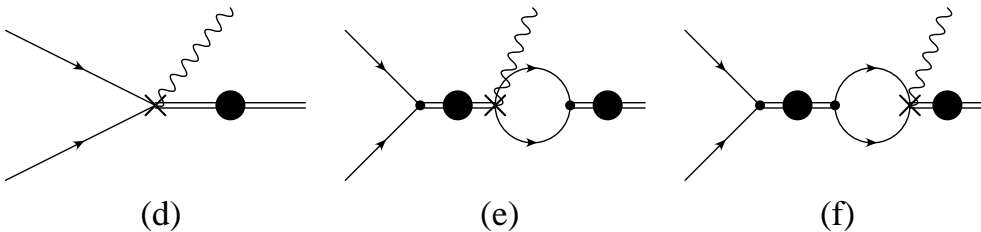


Figure 9: Higher order diagrams for the reaction $np \rightarrow d\gamma$ involving the $VdNN$ vertex coming from L'_1 . The order of diagrams is of $Q^{5/2}$.

Comparing the amplitudes in Eqs. (40) and (35), one finds that the momentum dependences of the amplitudes for the LEC's L_1 and L'_1 are slightly different. This difference, however, does not affect the numerical results at small energies significantly. Here we compute the M1 transition contribution to the $np \rightarrow d\gamma$ cross section, using two sets of the parameters: $\delta L_1 = 0.736$ fm and $L'_1 = 0$, and $\delta L_1 = 0$ and $L'_1 = 4.464$ fm $^{5/2}$; these LEC's have been fixed from σ^{exp} . Predictions for the $np \rightarrow d\gamma$ cross section at energies higher than the thermal neutron energy are given in Tab. 2 up to 1 MeV. A fairly good agreement is seen between the results corresponding to the two different choices of the parameter set. Our dEFT results also show reasonable agreement with the recent EFT calculations [27, 28], as well as with the accurate potential model calculation including the exchange current [29].

5. Discussion and conclusions

In this paper we have reexamined dEFT without pions for the deuteron reactions involving the electromagnetic (EM) probe. The EM form factors of the deuteron and the total cross sections of the $np \rightarrow d\gamma$ reaction have been calculated. We have found that the LEC's of the Vdd vertices in dEFT give much larger contributions than the corresponding term in the “usual” EFT approach (within the PDS scheme) that does not include the dibaryon fields. Although no formally rigorous methods exist to restore a proper counting rule in dEFT, we have proposed a practical prescription to extract the LO part of the LEC's in such manner that this LO part mimics the leading one-body VNN vertices. After the LO part is removed, the remainder is considered to represent the high energy physics that has been integrated out. If one is to calculate it explicitly, one should take into account relativistic corrections, meson-exchange currents, higher partial waves, *etc.* However, an easy way to fix the higher order part of the LEC's is to fit it to experimental data. We were able to confirm that the higher order corrections defined this way are indeed small in conformity with the general tenet of EFT.

With the LEC's thus determined, we have calculated the form factors $A(q)$ and $B(q)$ for elastic e - d scattering and found that the results of $A(q)$ are very close to the experimental data for momenta up to 200 MeV. Furthermore, our results of $A(q)$ and $B(q)$ are comparable to those of the accurate potential model calculation. Our estimations of the

E(MeV)	$\sigma_{M1}(\delta L_1)$	$\sigma_{M1}(L'_1)$	$\sigma_{M1}(EFT)[28]$	$\sigma_{M1}(Av18)[29]$
1.264×10^{-8}	334.2*	334.2*	334.2*	334.2*
5×10^{-4}	1.668	1.668	1.667	1.668
1×10^{-3}	1.171	1.171	1.170	1.171
5×10^{-3}	0.4953	0.4954	0.4950	0.4954
1×10^{-2}	0.3281	0.3281	0.3279	0.3281
5×10^{-2}	0.09814	0.09820	0.09810	0.09820
0.100	0.04969	0.04976	0.04973	0.04975
0.500	0.00775	0.00782	0.00787	0.00781
1.00	0.0035	0.0036	0.0036	0.00355

Table 2: M1 transition contribution to the cross sections for the $np \rightarrow d\gamma$ reaction. The second and third columns are our dEFT results using the two sets of LEC's described in the text. The fourth column shows the results of the NNLO EFT calculation[28], while the fifth column gives the results of an accurate potential model calculation (Av18) including the exchange current[29]. The LEC's in both dEFT and EFT and the strength of the exchange current in the potential model calculation are fixed at the values marked by *.

total cross sections of the $np \rightarrow d\gamma$ reaction for energies up to 1 MeV also agree well with the results of the other EFT calculations and the accurate potential model. The fact that, with the proper treatment of the LEC's in the Vdd vertices, the effective convergence of the dEFT expansion is restored, is interpreted as an indication that dEFT is a useful tool for understanding a wide class of low-energy phenomena involving the deuteron.

Acknowledgments

We thank S. Nakamura for providing us his numerical results in Table 1 and communications. We also thank K. Kubodera for reading the manuscript. S.A. thanks W. Detmold, J.-W. Chen, A. Parreno, P. F. Bedaque, S. R. Beane, T. Sato, F. Myhrer, H. W. Fearing, and M. J. Savage for discussions and communications. This work is supported in part by the Natural Sciences and Engineering Research Council of Canada and by the Korea Research Foundation (Grant No. KRF-2003-070-C00015).

Appendix

In this appendix we rederive the two-nucleon(dibaryon) propagators and fix the LEC's using the known properties of NN systems in the S -wave channels; see also Ref. [12].

The LO diagrams for the two-nucleon(dibaryon) propagators in the S -wave channels are depicted in Fig. 10. Since the insertion of the two-nucleon one-loop diagram does not alter the order of the diagram [5], the two-nucleon bubbles in the propagators should be summed up to infinite order. Thus the inverse two-nucleon(dibaryon) propagators in the

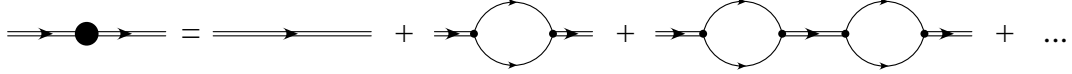


Figure 10: Diagrams for the two-nucleon(dibaryon) propagator at leading order: a double (single) line stands for the dibaryon (nucleon) field.

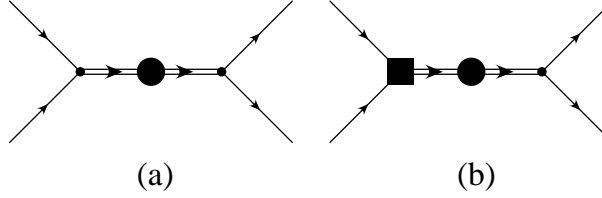


Figure 11: Diagrams for the NN scattering amplitudes. Diagram (a) is for S - to S -wave channel and diagram (b) is for D - to S -wave channel. The dNN vertex with (without) a filled box denotes a vertex proportional to $C_2^{(sd)}(y_{t,s})$. The propagator of the two-nucleon(dibaryon) field (a double line with a filled circle) is obtained from the diagrams in Fig. 10.

center-of-mass (CM) frame read

$$\begin{aligned} iD_{t,s}^{-1}(p) &= i\sigma_{t,s}(E + \Delta_{t,s}) + iy_{t,s}^2 \frac{m_N}{4\pi}(\mu + ip) \\ &= i \frac{m_N y_{t,s}^2}{4\pi} \left[\frac{4\pi\sigma_{t,s}\Delta_{t,s}}{m_N y_{t,s}^2} + \mu + \frac{4\pi\sigma_{t,s}E}{m_N y_{t,s}^2} + ip \right], \end{aligned} \quad (41)$$

where μ is the PDS scale, p is the magnitude of the nucleon momentum in the CM frame, and E is the total energy $E \simeq p^2/m_N$.

The two-nucleon(dibaryon) propagator in the spin singlet state, $D_s(p)$, can be renormalized using the 1S_0 channel NN scattering amplitude.⁸ The amplitude obtained from Fig. 11 (a) reads

$$i\mathcal{A}_s = (-iy_s)(iD_s(p))(-iy_s) = \frac{4\pi}{m_N} \frac{1}{\frac{4\pi\sigma_s\Delta_s}{m_N y_s^2} - \mu - \frac{4\pi\sigma_s}{m_N^2 y_s^2} p^2 - ip}, \quad (42)$$

and it is related to the S -matrix via

$$S - 1 = e^{2i\delta_0} - 1 = \frac{2ip}{p \cot\delta_0 - ip} = i \left(\frac{pm_N}{2\pi} \right) \mathcal{A}_s, \quad (43)$$

⁸Although it is known that the expansion series of the ERT parameters in the 1S_0 channel converges well, we adapt the modified counting rule $Q \sim \{p, a_0^{-1}, r_0^{-1}\}$ for the 1S_0 channel as well.

where δ_0 is the phase shift for the 1S_0 channel. Meanwhile effective range expansion (ERE) reads

$$p \cot \delta_0 = -\frac{1}{a_0} + \frac{1}{2} r_0 p^2 + \dots, \quad (44)$$

where a_0 ($= -23.71$ fm) is the scattering length and r_0 ($= 2.73$ fm) the effective range in the 1S_0 channel. Inserting Eq. (44) into Eq. (43), one obtains $\sigma_s = -1$, and

$$y_s = \frac{2}{m_N} \sqrt{\frac{2\pi}{r_0}}, \quad D_s(p) = \frac{m_N r_0}{2} \frac{1}{\frac{1}{a_0} + ip - \frac{1}{2} r_0 p^2}. \quad (45)$$

Now we fix the LEC's in the coupled channel. Diagrams for the ${}^3S_1 - {}^3D_1$ channel are depicted in Figs. 11 (a, b). Each of the amplitudes reads

$$\mathcal{A}_{[SS]} = \frac{4\pi}{m_N} \frac{1}{\frac{4\pi\sigma_t\Delta_t}{m_N y_t^2} - \mu - \frac{4\pi\sigma_t}{m_N^2 y_t^2} p^2 - ip}, \quad (46)$$

$$\mathcal{A}_{[DS]} = \frac{\sqrt{2}}{3} \frac{C_2^{(sd)} p^2}{y_t \sqrt{m_N \rho_d} m_N} \frac{4\pi}{\frac{4\pi\sigma_t\Delta_t}{m_N y_t^2} - \mu - \frac{4\pi\sigma_t}{m_N^2 y_t^2} p^2 - ip}. \quad (47)$$

The relation between the S -matrix and the amplitudes in the coupled channel is given by

$$S = 1 + i \frac{pm_N}{2\pi} \begin{pmatrix} \mathcal{A}_{[SS]} & \mathcal{A}_{[DS]} \\ \mathcal{A}_{[SD]} & \mathcal{A}_{[DD]} \end{pmatrix} = \begin{pmatrix} e^{2i\bar{\delta}_0} \cos 2\bar{\epsilon}_1 & ie^{i(\bar{\delta}_0 + \bar{\delta}_2)} \sin 2\bar{\epsilon}_1 \\ ie^{i(\bar{\delta}_0 + \bar{\delta}_2)} \sin 2\bar{\epsilon}_1 & e^{2i\bar{\delta}_2} \cos 2\bar{\epsilon}_1 \end{pmatrix}, \quad (48)$$

where we have employed a convention for the phase shifts defined in Ref. [30].

Since it is known that $\bar{\epsilon}_1$ is numerically small, we put $\cos(2\bar{\epsilon}_1) \simeq 1$. Around the deuteron pole, ERE reads [31],

$$p \cot \bar{\delta}_0 = -\gamma + \frac{1}{2} \rho_d (p^2 + \gamma^2) + \dots, \quad (49)$$

with $\gamma^{-1} = 4.319$ fm and $\rho_d = 1.764$ fm. Following the same steps that lead to Eq. (45), one obtains $\sigma_t = -1$, and

$$y_t = \frac{2}{m_N} \sqrt{\frac{2\pi}{\rho_d}}, \quad D_t(p) = \frac{m_N \rho_d}{2} \frac{1}{\gamma + ip - \rho_d \frac{1}{2} (\gamma^2 + p^2)} = \frac{Z_d}{E + B} + \dots, \quad (50)$$

where Z_d is the wave function normalization factor of the deuteron around the pole of the deuteron binding energy B , and the ellipsis in Eq. (50) denotes corrections that are finite or vanish at $E = -B$. Thus one obtains [12]

$$Z_d = \frac{\rho_d \gamma}{1 - \rho_d \gamma}. \quad (51)$$

Next we renormalize the coupled channel amplitude $\mathcal{A}_{[DS]}$ at the deuteron pole $p = i\gamma$ through the relation,

$$-2 \left(\frac{\eta_{sd}}{1 - \eta_{sd}^2} \right) = \frac{\tan(2\bar{\epsilon}_1)}{\sin(\bar{\delta}_0 - \bar{\delta}_2)} \Big|_{p=i\gamma} = \frac{2\mathcal{A}_{[SD]}}{\mathcal{A}_{[SS]} - \mathcal{A}_{[DD]}} \Big|_{p=i\gamma} \simeq -\frac{1}{3} \sqrt{\frac{m_N}{\pi}} C_2^{(sd)} \gamma^2, \quad (52)$$

where we have neglected the D -wave amplitude $\mathcal{A}_{[DD]}$. Thus, neglecting the η_{sd}^2 correction in the relation above, one obtains

$$C_2^{(sd)} \simeq 6 \sqrt{\frac{\pi}{m_N}} \frac{\eta_{sd}}{\gamma^2}. \quad (53)$$

References

- [1] S. Weinberg, hep-th/9702027.
- [2] S. Weinberg, Phys. Lett. **B 251** (1990) 288.
- [3] T.-S. Park, K. Kubodera, D.-P. Min and M. Rho, Nucl. Phys. **A 646** (1999) 83.
- [4] C. H. Hyun, T.-S. Park and D.-P. Min, Phys. Lett. **B 473** (2000) 6.
- [5] D. B. Kaplan, M. J. Savage and M. B. Wise, Phys. Lett. **B 424** (1998) 390.
- [6] S. R. Beane *et al.*, in (ed.) M. Shifman, *At the frontier of particle physics*, Vol.1 133, World Scientific, Singapore (2001); nucl-th/0008064.
- [7] P. F. Bedaque and U. van Kolck, Ann. Rev. Nucl. Part. Sci. **52** (2002) 339.
- [8] M. Rho, AIP Conf. Proc. **494** (1999) 391; nucl-th/9908015.
- [9] D. R. Phillips and T. D. Cohen, Nucl. Phys. **A 668** (2000) 45.
- [10] D. R. Phillips, G. Rupak, and M. J. Savage, Phys. Lett. **B 473** (2000) 209.
- [11] D. B. Kaplan, Nucl. Phys. **B 494** (1997) 471.
- [12] S. R. Beane and M. J. Savage, Nucl. Phys. **A 694** (2001) 511.
- [13] J. F. Beacom and S. J. Parke, Phys. Rev. D 64 (2001) 091302.
- [14] S. Ando, H. W. Fearing, V. Gudkov, K. Kubodera, F. Myhrer, T. Sato, and S. Nakamura, Phys. Lett. B 595 (2004) 250, nucl-th/0402100.
- [15] W. Detmold and M. J. Savage, hep-lat/0403005.
- [16] D. R. Phillips, Phys. Lett. **B 567** (2003) 12.
- [17] D. B. Kaplan, M. J. Savage, and M. B. Wise, Phys. Rev. C **59** (1999) 617.
- [18] J.-W. Chen, G. Rupak, and M. J. Savage, Nucl. Phys. **A 653** (1999) 386.
- [19] J.-W. Chen, X. Ji, and Y. Li, nucl-th/0407019.
- [20] N. Fettes, U.-G. Meißner, M. Mojžiš, and S. Steininger, Annals. Phys. **283** (2000) 273; Erratum *ibid.* **288** (2001) 249.

- [21] P. Mergell *et al.*, Nucl. Phys. **A 596** (1996) 367.
- [22] V. Z. Jankus, Phys. Rev. **102** (1956) 1586.
- [23] G. G. Simon, Ch. Schmitt, and V. H. Walther, Nucl. Phys. **A 364** (1981) 285.
- [24] T.-S. Park, D.-P. Min and M. Rho, Phys. Rev. Lett. **74** (1995) 4153
- [25] M. J. Savage, K. A. Scaldeferri, and M. B. Wise, Nucl. Phys. **A 652** (1999) 273.
- [26] A. E. Cox, S. A. R. Wynchank and C. H. Colli, Nucl. Phys. **74** (1965) 497.
- [27] J.-W. Chen and M. J. Savage, Phys. Rev. C **60** (1999) 065205.
- [28] G. Rupak, Nucl. Phys. **A 678** (2000) 405.
- [29] S. Nakamura, T. Sato, V. Gudkov, K. Kubodera, Phys. Rev. C **63** (2001) 034617.
- [30] H. P. Stapp, T. J. Ypsilantis, and N. Metropolis, Phys. Rev. **105** (1957) 302.
- [31] H. A. Bethe, Phys. Rev. **76** (1949) 38.